Hindawi
Advances in Civil Engineering
Volume 2018, Article ID 1368965, 13 pages
https://doi.org/10.1155/2018/1368965

Research Article

Research on Deformation Mechanism of Retracement Channel during Fully Mechanized Caving Mining in Superhigh Seam

Liu Fei[1] **and Zhongxi Jiang**[2]

[1]*National Engineering Research Center of Coal Mine Water Hazard Controlling, Suzhou University, Suzhou 234000, China*
[2]*Shenzhen Research Institute, Shanghai Jiao Tong University, Shenzhen 518057, China*

Correspondence should be addressed to Zhongxi Jiang; s11jzx@163.com

Received 20 September 2018; Accepted 21 November 2018; Published 24 December 2018

Guest Editor: Jian Sun

The multichannel retracement in the auxiliary laneway has become one of the key technologies in the high-yield and high-efficiency production of large and extra-large coal mines in western China. For the successful application of this technology, the control of retracement channel deformation is decisive. This paper takes the support of the retracement channel in full-mechanized caving working surface of Mentai Buliangou Coal Mine as the engineering background. In view of the occurrence characteristics of thin bedrock, thick unconsolidated layer and superhigh seam, theoretical analysis, numerical calculation, and field industrial test are adopted. The deformation rules and stress distribution characteristics of the surrounding rock as well as the changes of the support structure in the retracement channel during the end mining on the full-mechanized caving working surface are systematically studied, and the deformation and failure mechanism of the surrounding rock is revealed. The field measurement shows that the adoption of optimal design scheme can effectively control the deformation of the surrounding rock in the retracement channel during the end mining period and consequently address the problem of rapid moving of the working surface, which is significant for engineering practices.

1. Introduction

At present, coal is one of China's major energy sources, accounting for about 60% of nonrenewable energy production and consumption [1–3], of which thick coal seam production accounts for about 45% of total raw coal output. The continuously improved technology of full-mechanized caving mining has become an effective way to tackle the thick coal seam mining and achieve mining safety and high yield [4–8]. Traditionally, the moving of working surface in fully mechanized coal mining (caving) in China is realized through the channel opening of coal cutters. During the last cuttings near the stop line of the working surface, the coal cutter and the transport machine move forward to cut the coal, with the bracket remaining in its original position, thus forming space for equipment to turn and retrace. In the past, the working surface moving through single-channel or coal cutter self-retaining channel in large and extra-large coal mines in China took about three months or longer, which greatly restricts the moving speed [9].

As early as the beginning of 1970s, the United States took the lead in the use of rapid moving equipment and advanced moving process for fully mechanized coal mining (caving) working surface, which formed a complete set of technology covering the moving of the old surface and the installation of the new one and shortened the moving time to about one week. In recent years, with the successful application of such complete sets of rapid moving equipment in the United States, multipoint and single-point retreat processes have been gradually developed in mining areas according to their geological conditions. The

increasingly mature moving technology has been extensively applied in coal mining countries such as Australia and South Africa [10–14] and has achieved significant economic and social benefits in these countries. In the 1990s, China's Shendong mining area first introduced the technology for rapid moving of the working surface in fully mechanized coal mining (caving). In addition, based on the imported rapid moving process, the new moving technology of "multichannel in auxiliary laneway" was studied by Shendong mining area. The successful practice of this new technology in the mine area marked a new breakthrough in the rapid moving of fully mechanized coal mining (caving) equipment in China, which achieved great development later [15, 16]. With the continuous improvement of domestic fully mechanized coal mining (caving) technology, advanced multichannel retracement in the auxiliary laneway has been adopted in many large mining areas in Shendong and Ningxia. In this process, two auxiliary laneways are excavated parallel to the backstopping working surface while digging the two roadways at the stop line of the backstopping working surface. The channel on the side of the working surface is called the main retracement laneway, and the one on the side of the main roadway is called the assistant retracement laneway. 4 to 6 connecting lanes are provided between the two channels, forming a multichannel system in the auxiliary laneway. This kind of working surface moving technology based on multichannel in auxiliary laneway can realize the simultaneous relocation of fully mechanized coal mining (caving) equipment in 4–6 connecting lanes. According to statistics, it took only 10 days for the Shendong mining area to move its old working surface and install the new one through this technology, and the similar process in the Yujialiang Coal Mine 45101 took only 6 days and 23 hours. Compared with the previous moving of working surface in coal cutter self-retaining channel, this new technology significantly shortened the moving time (nearly 90% to the most) and effectively ensured the efficient production in mines [17–22]. The Mentai Buliangou Coalfield, located on the Loess Plateau of Ordos, features a typical Loess Plateau landform [23], with complex landscape, interlaced ravines, and well-developed dendritic gullies. In addition, complex geological conditions such as thin bedrock and superhigh seam [24–26] lead to a series of mining problems, including severe deformation of rock surrounding the working surface (Figure 1) and increased pressure on the advanced support in laneway. At present, in-depth studies on the deformation mechanism of the retracement channel under special geological conditions in the west are few; therefore, research studies on the deformation mechanism of retracement channel in thin bedrock, thick unconsolidated layer, and superhigh seam and the deformation control solutions will be helpful to guide the improving of working surface rapid moving, which is significant for engineering practices and will provide reference for the implementation of rapid moving of fully mechanized caving workface in similar mines.

2. Engineering Geological Conditions

Mentai Buliangou Coalfield is located in the Loess Plateau of Ordos (Figure 2). It is a typical Loess Plateau landform with complex topography, vertical and horizontal ravines, and well-developed dendritic gullies. The strike length of No. 201 working face in Mentai Buliangou Coal Mine is 1 395 m, the inclined length is 240.3 m, the average thickness of coal seam is 16 m, the inclination angle of coal seam is 0–8 degree, the average depth is 4 degree, and the average mining depth is 295 m. Detailed lithological descriptions of the rock strata are illustrated in Figure 3.

3. Establishment of Mechanical Model for Retracement Channel

The retracement channel is a kind of laneway specially excavated for the moving of fully mechanized coal mining (caving) working surface, and the quality of its support determines whether the working surface equipment can be removed smoothly. The establishment of a mechanical model (Figure 4) and the theoretical analysis of the surrounding rock stability created a basis for the deformation control and safe operation of the retracement channel.

When the working surface is connected with the main retracement channel, the simplified model is a rectangular section beam supported at one end. "q_1" is the simplified uniform load of the overlying rock; "a" is the width of the assistant retracement channel; "b" is the distance between the plastic zone of coal pillar and the major wall of the assistant retracement channel; "c" is the distance between the plastic zone of the minor wall of main retracement channel and the major wall of the assistant retracement channel; "d" is the distance between the minor wall of the main retracement channel and the major wall of the assistant retracement channel; "h" is the height of the beam, "l" is the total length of the beam, and q_2 is the simplified uniform load of plastic zone of the minor wall of assistant retracement channel; q_3 is the simplified uniform load of plastic zone of the minor wall of main retracement channel; "e" is the total length of the main retracement channel and the working surface hydraulic bracket; q_4 is the simplified uniform load of the bracket. The deflection is calculated by

$$EI\omega'' = M(x). \tag{1}$$

The bending moment in the model is divided into the following five segments for calculation:

(1) $d < x \le l$:

$$M_5(x) = \int_x^l (\xi - x)(q_1 - q_4)d\xi. \tag{2}$$

(2) $c < x \le d$:

$$M_4(x) = \int_x^d (\xi - x)\left[q_1 - \frac{q_3(d-\xi)}{(d-c)}\right]d\xi + M_5|_{x=d} + (q_1 - q_4)(l-d)(d-x). \tag{3}$$

Figure 1: Large deformation of roadway in Mentai Buliangou Coalfield.

Figure 2: Location of the Mentai Buliangou Coal Mine, Inner Mongolia, China.

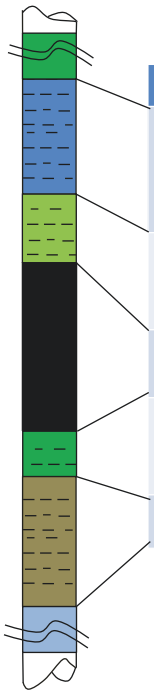

Thickness (m)	Lithology	Lithology description
11.8	Coarse mudstone and sandy mudstone	Coarse sandstone: gray white, thick layered; sandy mudstone: black brown, thin muddy structure.
2.6	Mudstone and sandy mudstone	Sandy mudstone: dark brown, thin muddy structure; mudstone: gray, black, layered structure.
16	Coal	Black, joint and fissure development
3.2	Mudstone and sandy mudstone	Mudstone: grey, thin layer; sandy mudstone: grey, muddy structure.
15.5	Coarse sand rock	Gray white, thick layered

Figure 3: Stratigraphic column and geological description.

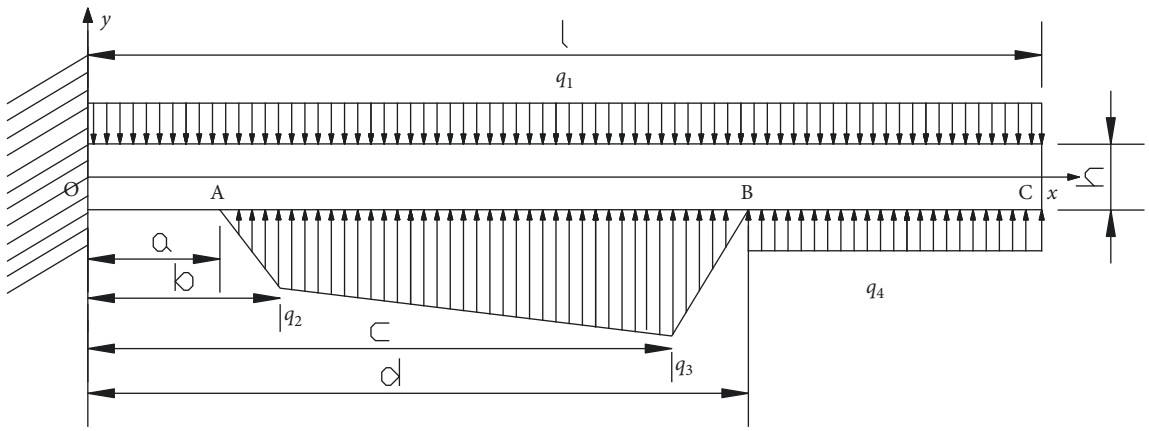

Figure 4: Simplified mechanical model for retracement channel.

(3) $b < x \le c$:

$$M_3(x) = \int_x^c (\xi - x)\left[q_1 - \left[\frac{q_3 - q_2}{c-b}(\xi - b) + q_2\right]\right]d\xi + M_4|_{x=c} + (c-x)\left[q_1(l-c) - \frac{q_3}{2}(d-c) - q_4(l-d)\right]. \tag{4}$$

(4) $a < x \le b$:

$$M_2(x) = \int_x^b (\xi - x)\left[q_1 - \frac{q_2(\xi - a)}{b-a}\right]d\xi + M_3|_{x=b} + (b-x)\left[q_1(l-b) - q_4(l-d) - \frac{q_3(d-c)}{2} - \frac{(q_2+q_3)(c-b)}{2}\right]. \tag{5}$$

(5) $0 < x \le a$:

$$M_1(x) = \int_x^a (\xi - x)q_1 d\xi + M_2|_{x=a} + (a-x)\left[q_1(l-a) - q_4(l-d) - \frac{q_3(d-c)}{2} - \frac{(q_2+q_3)(c-b)}{2} - \frac{q_2(b-a)}{2}\right] + M_2|_{x=a}. \tag{6}$$

The bending moments of the five segments were obtained from equations (2)–(6):

(1) $d < x \le l$:

$$M_5(x) = \frac{1}{2}l^2q_1 - \frac{1}{2}l^2q_1 - \frac{1}{2}l^2q_4 - xlq_1 + xlq_4 + \frac{1}{2}x^2q_1 - \frac{1}{2}x^2q_4. \tag{7}$$

(2) $c < x \le d$:

$$M_4(x) = \frac{1}{2}\frac{-6q_4d^2 + 3l^2q_4c + 3x^2q_1d - 3d^2q_4c + 3l^2q_1d - 3l^2q_4d - 3l^2q_1c - 3x^2q_1c - 3x^2q_3d}{d-c} + \frac{1}{2}\frac{6q_4dxc - 6xlq_4c + 6xlq_4d + 6xlq_1c - 6xlq_1d + 3d^2xq_3 + x^3q_3 - q_3d^3 + 3d^2xq_3 + x^3q_3 - q_3d^3 + 3d^3q_4}{d-c}. \tag{8}$$

(3) $b < x \le c$:

$$M_3(x) = -\frac{1}{6}c\frac{(-2c^2q_3 - c^2q_2 + 3cq_3x + 3cq_2x + 3c^2q_1 - 3cq_1b + 3cbq_3 - 6xq_1c + 6xq_1b - 6xbq_3)}{b-c} - \frac{1}{6}x^2\frac{(-xq_3 + xq_2 + 3q_1c - 3q_1b + 3bq_3 - 3q_2c)}{b-c} + (c-x)\left[q_1(l-c) - \frac{1}{2}q_3(d-c) - q_4(l-d)\right] - \frac{1}{6}d\frac{(q_3d^2 - 3dcq_3 - 3d^2q_1 + 9dq_1c - 6q_1c^2)}{d-c} - \frac{1}{6}c^2\frac{(-cq_3 - 3q_1d + 3q_1c + 3q_3d)}{d-c} + (q_1 - q_4)(l-d)(d-c) + \frac{1}{2}l^2q_1 - \frac{1}{2}l^2q_4 - dlq_1 + dlq_4 + \frac{1}{2}d^2q_1 - \frac{1}{2}d^2q_4. \tag{9}$$

(4) $a < x \le b$:

$$M_2(x) = \frac{1}{6}b\frac{-2b^2q_2 + 3bxq_2 + 3q_1b^2 - 3bq_1a + 3bq_2a - 6xq_1b + 6xq_1a - 6xq_2a}{b-a} - \frac{1}{6}x^2\frac{(xq_2 - 3q_1b + 3q_1a - 3q_2a)}{b-a} + (b-a)\left[q_1(l-b) - q_4(l-d) - \frac{1}{2}q_3(d-c) - \frac{1}{2}(q_2+q_3)(c-b)\right] + \frac{1}{2}d^2q_4 - \frac{1}{6}q_3d^2 - dbq_4 + \frac{1}{2}bq_3d - \frac{1}{6}dcq_3 - \frac{1}{2}l^2q_4 + \frac{1}{2}l^2q_1 - \frac{1}{3}b^2q_3 + blq_4 - \frac{1}{6}c^2q_2 + \frac{1}{6}cbq_3 + \frac{1}{2}q_1b^2 + \frac{1}{3}cbq_2 - \frac{1}{6}b^2q_2 - blq_1. \tag{10}$$

(5) $0 < x \le a$:

$$M_1(x) = q_1a^2 - q_1xa + \frac{1}{2}x^2q_1 + (a-x)\left[q_1(l-a) - q_4(l-a) - \frac{1}{2}q_3(d-c) - \frac{1}{2}(q_2+q_3)(c-b) - \frac{1}{2}q_2(b-a)\right] + \frac{1}{6}b^2q_3 - \frac{1}{2}baq_3 + \frac{1}{6}cbq_3 + \frac{1}{6}bq_2a - \frac{1}{6}cbq_2 - \frac{1}{3}q_2a^2 - \frac{1}{6}q_3d^2 - aq_1l - aq_4d - \frac{1}{6}dcq_3 - \frac{1}{2}l^2q_4 + \frac{1}{2}aq_2c + \frac{1}{2}aq_3d + \frac{1}{2}d^2q_4 + aq_4l - \frac{1}{6}c^2q_2 + \frac{1}{2}l^2q_1. \tag{11}$$

Substituting $a = 5$ m, $b = 2.42$ m, $c = 15.15$ m, $d = 2.43$ m, $e = 5.5 + 8.6 = 14.1$ m, $h = 10$ m, $q_1 = \gamma H = 6.25$ MPa, $q_2 = 14.1$ MPa, $q_3 = 24.3$ MPa, $q_4 = 18.3$ MPa, and the elastic modulus 2.2 GPa of the Mentai Buliangou coal measured in laboratory into equations (7)–(11), we get the bending moments of segments, which are put into equation (1) for the angles and deflections of segments, shown in equations (12)–(21).

(1) Angle:

$$\theta_0(x, q_4) = \frac{-7.14.94x + 49.68x^2 - x^3 - 451.9q_4x + 7.05x^2q_4 + A_1}{EI}, \tag{12}$$

$$\theta_a(x, q_4) = \frac{-594.42x + 13.52x^2 - 0.24x^4 + 5.82x^3 - 451.9q_4x + 7.05x^2q_4 + A_2}{EI}, \tag{13}$$

$$\theta_b(x, q_4) = \frac{-943.36x + 84.06x^2 - 2.75 \times 10^{-2}x^4 - 0.52x^3 - 451.9q_4x + 7.05x^2q_4 + A_3}{EI}, \tag{14}$$

$$\theta_c(x, q_4) = \frac{7.05x^2q_4 - 451.9q_4x - 40.15x^3 - 21133.73x + 1425.9x^2 + 0.41x^4 + A_4}{EI}, \tag{15}$$

$$\theta_d(x, q_4) = \frac{4586.43x - 764.41q_4x - 117.3x^2 + 19.55x^2q_4 + x^3 - 0.17q_4x^3 + A_5}{EI}. \tag{16}$$

(2) Deflection:

$$w_0(x, q_4) = \frac{-357.47x^2 + 16.56x^3 + 0.25x^4 - 225.95x^2q_4 + 2.35q_4x^3 + A_1x + B_1}{EI}, \tag{17}$$

$$w_a(x, q_4) = \frac{-297.21x^2 + 4.51x^3 - 4.82 \times 10^2x^5 + 1.46x^4 - 225.95x^2q_4 + 2.35q_4x^3 + A_2x + B_2}{EI}, \tag{18}$$

$$w_b(x, q_4) = \frac{-471.68x^2 + 28.02x^3 - 5.5 \times 10^{-3}x^5 - 0.136x^4 - 225.95x^2q_4 + 2.35q_4x^3 + A_3x + B_3}{EI}, \tag{19}$$

$$w_c(x, q_4) = \frac{2.35q_4x^3 - 225.95x^2q_4 - 10.04x^4 - 10566.87x^2 + 475.3x^3 + 8.23 \times 10^{-2}x^5 + A_4x + B_4}{EI}, \tag{20}$$

$$w_d(x, q_4) = \frac{2293.22x^2 - 382.2x^2q_4 - 39.1x^3 + 6.52q_4x^3 + 0.25x^4 - 4.17 \times 10^{-2} + A_5x + B_5}{EI}. \tag{21}$$

The continuity condition of the beam is

$$\begin{cases} \omega'(0) = 0, \\ \omega(0) = 0, \end{cases}$$
$$\begin{cases} \omega'(5)_{\text{left}} = \omega'(5)_{\text{right}}, \\ \omega(5)_{\text{left}} = \omega(5)_{\text{right}}, \end{cases}$$
$$\begin{cases} \omega'(7.42)_{\text{left}} = \omega'(7.42)_{\text{right}}, \\ \omega(7.42)_{\text{left}} = \omega(7.42)_{\text{right}}, \end{cases} \quad (22)$$
$$\begin{cases} \omega'(22.57)_{\text{left}} = \omega'(22.57)_{\text{right}}, \\ \omega(22.57)_{\text{left}} = \omega(22.57)_{\text{right}}, \end{cases}$$
$$\begin{cases} \omega'(25)_{\text{left}} = \omega'(25)_{\text{right}}, \\ \omega(25)_{\text{left}} = \omega(25)_{\text{right}}. \end{cases}$$

Substituting EI and equations (12)–(21) into the continuity condition of the beam, we get

$$\begin{aligned} w_0(x, q_4) &= -9.03 \times 10^{-3}x^2 + 4.18 \times 10^{-4}x^3 + 6.31 \times 10^{-6}x^4 \\ &\quad - 5.71 \times 10^{-3}x^2 q_4 + 5.93 \times 10^{-5} q_4 x^3, \\ w_a(x, q_4) &= -7.5 \times 10^{-3}x^2 + 1.14 \times 10^{-4}x^3 - 1.22 \times 10^{-6}x^5 \\ &\quad + 3.67 \times 10^{-5}x^4 - 5.71 \times 10^{-3}x^2 q_4 \\ &\quad + 5.93 \times 10^{-5} q_4 x^3 - 3.8 \times 10^{-3}x + 3.8 \times 10^{-3}, \\ w_b(x, q_4) &= -1.19 \times 10^{-2}x^2 + 7.07 \times 10^{-4}x^3 - 1.39 \times 10^{-7}x^5 \\ &\quad - 3.26 \times 10^{-6}x^4 - 5.71 \times 10^{-3}x^2 q_4 \\ &\quad + 5.93 \times 10^{-5} q_4 x^3 + 1.25 \times 10^{-2}x - 2.05 \times 10^{-2}, \\ w_c(x, q_4) &= 5.93 \times 10^{-5} q_4 x^3 - 5.71 \times 10^{-3}x^2 q_4 \\ &\quad - 2.53 \times 10^{-4}x^4 - 0.27x^2 + 1.2 \times 10^{-10}x^3 \\ &\quad + 2.08 \times 10^{-6}x^5 + 2.89x - 13 + 2.5 \times 10^{-19} q_4, \\ w_d(x, q_4) &= 5.79 \times 10^{-2}x^2 - 9.65 \times 10^{-3}x^2 q_4 \\ &\quad - 9.87 \times 10^{-4}x^3 + 1.65 \times 10^{-4} q_4 x^3 \\ &\quad + 6.31 \times 10^{-6}x^4 - 1.05 \times 10^{-6} q_4 x^4 \\ &\quad + 6.58 \times 10^{-2} q_4 x - 1.17x - 0.41 q_4 + 7.29. \end{aligned} \quad (23)$$

The deflection curve of main retracement channel when q4 is 0.6 MPa, 0.7 MPa, and 0.8 MPa is shown in Figure 5.

The initial support force of the hydraulic bracket of the working surface in Mentai Buliangou Coal Mine is 0.7 MPa. According to the actual conditions, the maximum deformation of the main retracement channel under that support force was calculated as 561 mm, which meets the requirements for the working surface moving in the main retracement channel.

4. Finite Element Method Simulation

4.1. Establishment of Mechanical Calculation Model. Based on the geological conditions and the actual mining practices in Mentai Buliangou Coal Mine, a calculation model was established as 100 m wide, 170 m long, and 66 m high. The main retracement laneway is 5.5 m, the assistant retracement laneway is 5 m, and the coal pillar between them is 20 m.

In the model, the mining in the "y" direction was only 60 m, leaving a 40 m protection boundary. The main and assistant retracement channels were excavated before backstopping the working surface. Advancing 10 m at a time, the simulated excavation during backstopping was 100 m. Caving was used for the first 70 m and not for the 30 m from the main retracement channel, thus the mining height was 3.8 m. The deformation characteristics and stress distribution of the rock surrounding the main and assistant retracement channels in different support parameters and different bolt and anchor pretightening forces were analyzed. The three-dimensional graphics of the model after the meshes around the main and assistant retracement channel were moderately densified and are shown in Figure 6.

4.1.1. Model Boundary Conditions. According to the actual conditions and the calculation model, the model boundary conditions were stipulated as follows.

The top of the model was applied with the self-weight stress of the overlying rock; the lower boundary of the model was simplified as the displacement boundary condition, which was movable in the "x" direction and fixed in the "y" direction, i.e., $v = 0$; on both sides of the model was solid coal, which was simplified as the displacement boundary, movable in the "y" direction and fixed in the "x" direction, i.e., $u = 0$.

The self-weight stress σ_y was calculated in the equation $\sigma_y = \gamma H$. The average volume weight of the overlying rock γ was set at 25 N/m^3, H as the distance between the top of the established model to the ground, and the average buried depth of the Mentai Buliangou coal seam is 249.8 m. Therefore, the calculated result σ_y was about 62.5 MPa.

4.1.2. Model Yield Criterion. According to the field sampling and the rock mechanical test result, when the load reaches the strength limit [27, 28], the rock mass will be damaged, and the residual strength of rock mass will reduce gradually with the deformation development during peak plastic flowing. Therefore, the Mohr–Coulomb yield criterion was adopted during calculation to judge the fracture of rock mass.

4.1.3. Distribution of Rock. A total of 49.1 m rock stratum was taken as the model in the vertical direction, covering the lower bottom, direct bottom, coal seam, direct roof, and upper roof. From bottom to top: lower bottom 15.5 m, direct bottom 3.2 m, coal seam 16 m, direct roof 2.6 m, and upper roof 11.8 m. The rock mechanical parameters of each rock stratum are shown in Table 1.

4.2. Numerical Simulation Scheme Calculation. The deformation and stress distribution characteristics of the surrounding rock in the retracement channel during the end mining on the full-mechanized caving working surface in different support parameters were studied. According to the theoretical calculation results, the following three supporting schemes were selected for

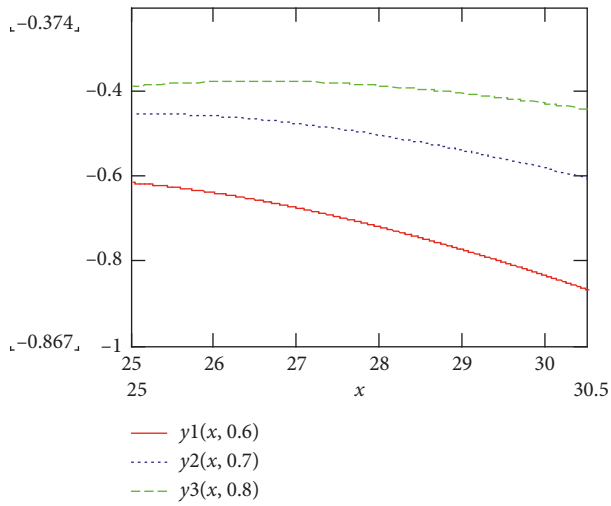

Figure 5: Main retracement channel deflection curve.

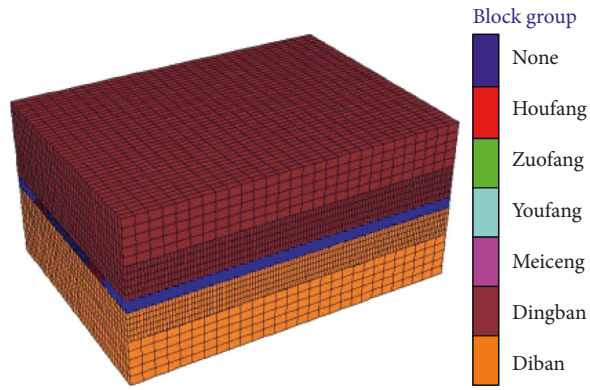

Figure 6: FLAC^{3D} schematic diagram.

Table 1: Rock mechanics parameters.

Lithology	Density d (kg·m^{-3})	Bulk modulus K (GPa)	Shear modulus G (GPa)	Bond strength σ (MPa)	Tensile strength σ (MPa)	Internal friction angle f
Coarse mudstone and sandy mudstone (main roof)	2458	17.65	8.52	3.22	9.53	32.60
Mudstone and sandy mudstone (immediate roof)	2155	8.53	12.37	1.69	4.96	30.85
Coal	1298	2.39	1.68	1.42	0.46	23.88
Mudstone and sandy mudstone (direct bottom)	2155	4.98	8.56	1.83	6.35	30.66
Coarse sand rock (old bottom)	2655	13.29	11.04	8.30	9.26	31.55

optimizing. The deformation and stress distribution of the surrounding rock of the retracement channel during the end mining on the working surface were calculated separately. The simulation scheme is shown in Table 2.

5. Numerical Results Analysis

5.1. Study on Displacement Distribution Law of Surrounding Rock in Retracement Channels. In order to analyze and compare the working surface effect on the retracement channel and the stability of the coal pillar and monitor the changes of the relative roof-to-floor convergence of the main and assistant retracement channels and the relative wall convergence during the advancement on the working surface, the changes in the process, curve graphs were developed as shown in Figures 7–12.

It can be seen from Figures 7–9 that as the working surface advanced forward, the roof-to-floor convergence and the wall convergence of the assistant retracement channel increased gradually. However, when the working surface advanced to 30 m of main retracement channel, the deformation of the retracement channel began to increase sharply due to the pressure of the working surface. Under the support condition in Scheme 3, when the working surface

Table 2: Supporting scheme.

	Bolt	Anchor cable	Spacing between bolts	Spacing between anchor cables	Bolt material	Anchor cable material
Scheme 1	Positive working slope: Φ20 × 2400 Side working slope: Φ20 × 2400 Roof: Φ20 × 2400	Φ17.8 × 8000	Positive working slope: 1000 × 1000 Side working slope: 1000 × 900 Roof: 1000 × 1000	1750 × 3000	Equal strength thread steel Equal strength thread steel Equal strength thread steel	Steel strand
Scheme 2	Positive working slope: Φ20 × 2400 Side working slope: Φ20 × 2400 Roof: Φ22 × 2500	Φ17.8×8000	Positive working slope: 900 × 900 Side working slope: 900×900 Roof: 1000 × 900	1750 × 2700	Equal strength thread steel Equal strength thread steel Equal strength thread steel	Steel strand
Scheme 3	Positive working slope: Φ20 × 2400 Side working slope: Φ20 × 2400 Roof: Φ22 × 2500	Φ17.8×8000	Positive working slope: 800 × 900 Side working slope: 800 × 900 Roof: 1000 × 900	1750 × 2700	Equal strength thread steel Equal strength thread steel Equal strength thread steel	Steel strand

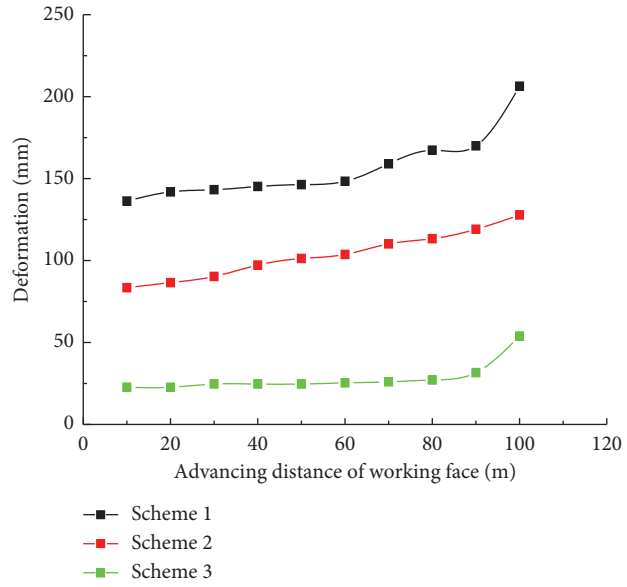

Figure 7: Assistant retracement channel: major wall deformation.

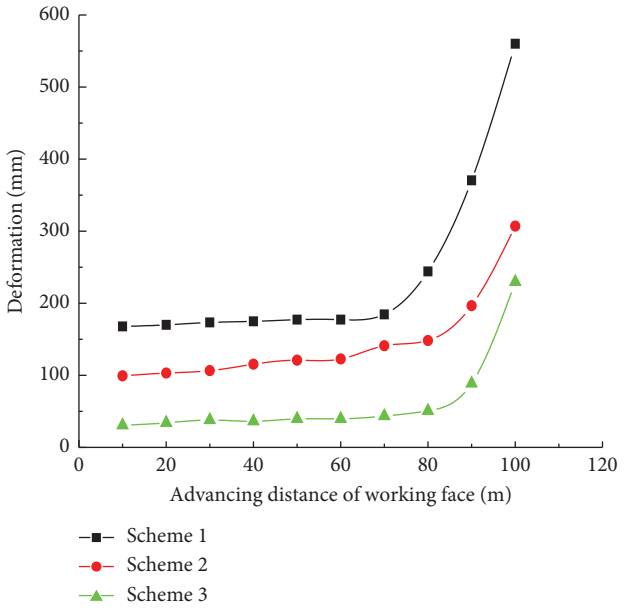

Figure 8: Assistant retracement channel: minor wall deformation.

advanced to 70 m, the maximum roof-to-floor convergence of the assistant retracement channel was 50.47 mm, the maximum deformation of the minor wall was 37.44 mm, and the maximum deformation of the major wall was 28.02 mm; when the working surface advanced to 80 m, the maximum roof-to-floor convergence of the assistant retracement channel was 53.71 mm, the deformation of the minor wall was 47.87 mm, and the deformation of the major wall was 30.01 mm; when the working surface advanced to 90 m, the maximum roof-to-floor convergence of the assistant retracement channel was 81.82 mm, the deformation of the minor wall was 85.13 mm, and the deformation of the major wall was 33.46 mm; when the working surface advanced to 100 m or cut through, the maximum roof-to-floor convergence of the assistant retracement channel was 236.73 mm, the deformation of the minor wall was 226.13 mm, and the deformation of the major wall was 55.67 mm. Under the same condition, Scheme 3, compared to Scheme 1, reduced the relative deformation between roof and floor by 70.9%, 72.6%, 70.3%, and 50.4%; reduced the deformation of minor wall by 79.2%, 80.1%, 76.9%, and 59.7%; and reduced the deformation of major wall by 82.4%, 82.1%, 80.9%, and 73.2%.

It can be seen from Figures 10–12 that as the working surface advanced forward, the roof-to-floor convergence and the wall convergence of the main retracement channel increased gradually. However, when the working surface advanced to 30 m from the main retracement channel, the

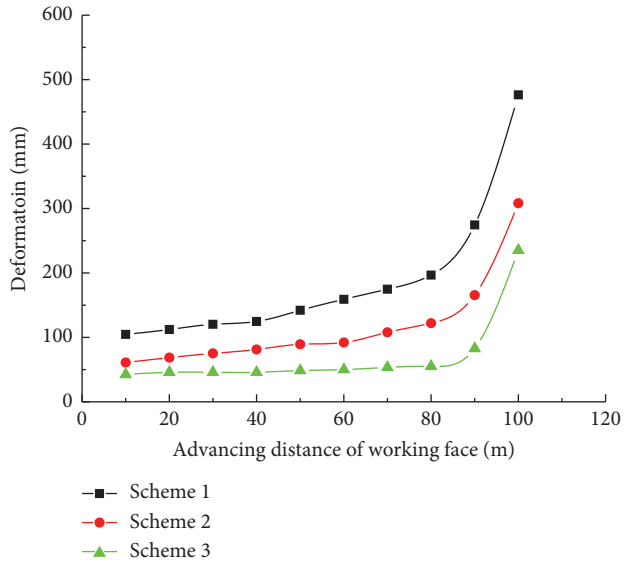

Figure 9: Relative deformation between the roof and floor of assistant retracement channel.

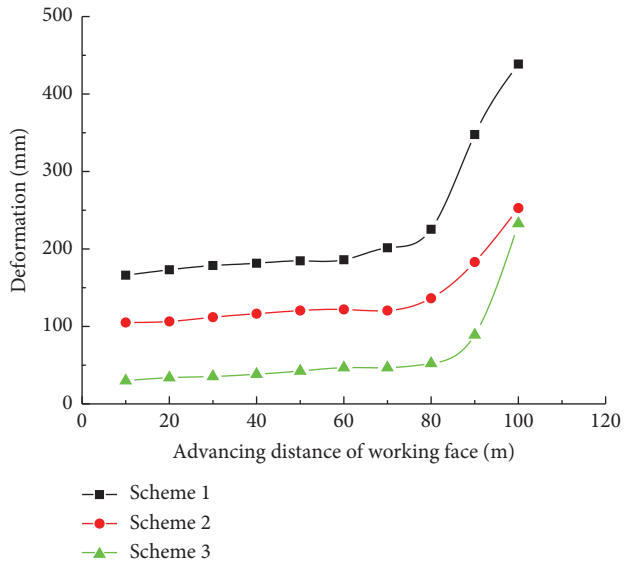

Figure 10: Main retracement channel: minor wall deformation.

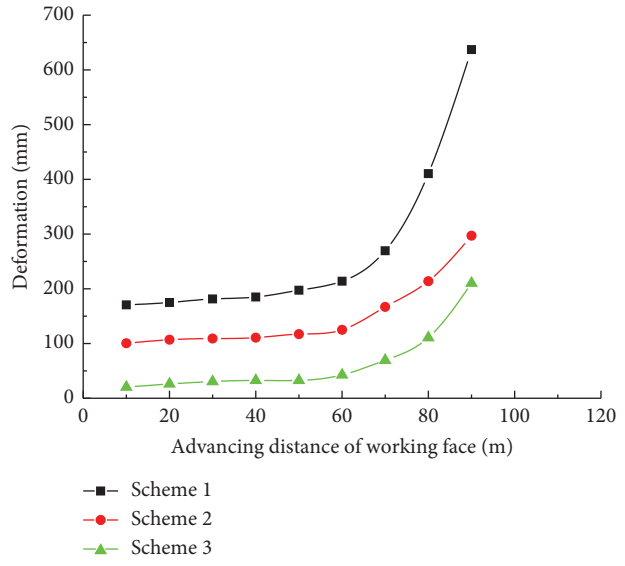

Figure 11: Main retracement channel: major wall deformation.

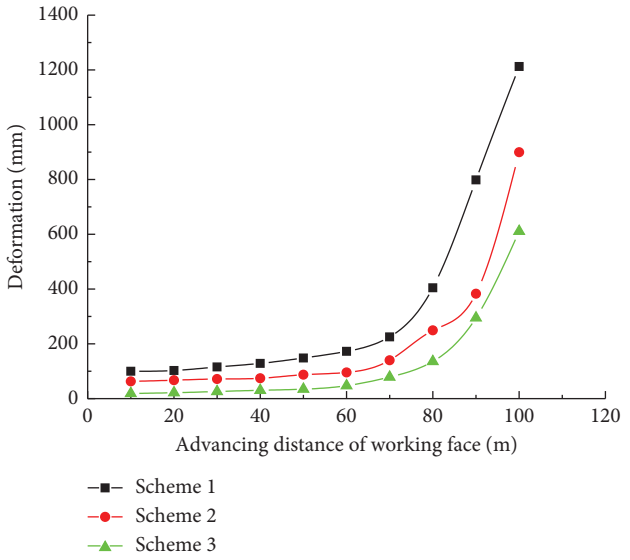

Figure 12: Relative deformation between the roof and floor of main retracement channel.

deformation of the retracement channel began to increase sharply due to the pressure of the working surface. When the working surface was penetrated, the deformation of the retracement channel reached the maximum. Under the support condition in Scheme 3, when the working surface advanced to 70 m, the maximum roof-to-floor convergence of the main retracement channel was 94.95 mm, the maximum deformation of the minor wall was 48.83 mm, and the maximum deformation of the major wall was 67.24 mm; when the working surface advanced to 80 m, the maximum roof-to-floor convergence of the main retracement channel was 141.86 mm, the deformation of the minor wall was 53.44 mm, and the deformation of the major wall was 108.33 mm; when the working surface advanced to 90 m, the maximum roof-to-floor convergence of the main retracement channel was 299.263 mm, the deformation of the minor wall was 91.04 mm, and the deformation of the major wall was 208.71 mm; when the working surface advanced to 100 m or cut through, the maximum roof-to-floor convergence of the main retracement channel was 615.86 mm and the deformation of the minor wall was 236.69 mm; under the same condition, Scheme 3, compared to Scheme 1, reduced the relative deformation between roof and floor by 58.9%, 65.4%, 62.6%, and 49.2%; reduced the deformation of the minor wall by 75.7%, 76.4%, 74%, and 46.4%; and reduced the deformation of the major wall by 74.9%, 73.6%, and 67.5%.

5.2. Study on Stress Distribution Law of Surrounding Rock in Retracement Channels. It can be seen from Figure 13 that the vertical stress in the coal pillars showed similar changing laws in different support schemes during the advancement of

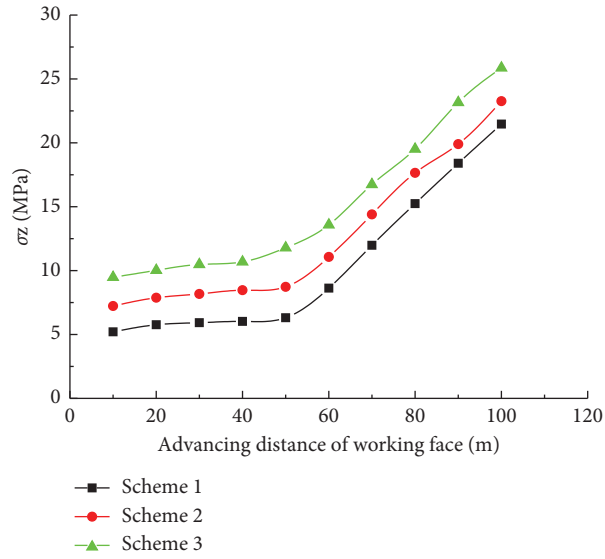

Figure 13: Vertical stress in protective coal pillars.

working surface: increased with the advancement. Under the support condition in Scheme 3, the vertical stress peak was the maximum, while under that in Scheme 1, the value was the minimum. The vertical stress under support condition in Scheme 3 was 26.1 MPa, 20.8% higher than Scheme 1. Analysis shows that the greater the support strength, the more integral the coal pillars and the greater the compressive strength. Under the influence of overlying strata pressure, the deformation reduced and the stress increased. To conclude, Scheme 3 is the most effective, followed by Scheme 2 and Scheme 1.

6. Retracement Channel Support Control Practices

6.1. Experimental Retracement Channel Support Conditions

Roof. Anchor specification: Φ22 × 2500 mm left-handed steel bolt without longitudinal reinforcement; 6 bolts in each row, row spacing: 1000 × 900 mm; each bolt is lengthened by one CK2350 and one Z2350 resin anchorage agent, with a dish-shaped steel tray: 150 × 150 × 10 mm; anchor row alternately matched with a steel ladder beam and steel band welded with 14 mm round steel. Reinforcing bar ladder and beam are covered with reinforcing steel mesh. Anchor cable specifications: Φ17.8 × 8000 mm steel strand anchor cable; each row of three, row spacing: 1750 × 2700 mm; each anchor cable using three Z2350 resin anchorage agent lengthened anchorage, with high-strength cable tray: 300 × 300 × 14 mm, a set of special locks. Concrete with top surface not less than 50 mm thick (as shown in Figures 14 and 15).

Coal Pillar Side. Bolt specifications: 20 ∗ 2500 mm right-handed full-thread steel bolt; each row of five, row spacing: 800 × 900 mm; each bolt using two Z2350 resin anchorage agent lengthened anchorage, with a dish-shaped steel pallet: 150 × 150 × 10 mm; each row of bolts with two steel ladder beams welded with 14 mm round steel, 1.9 m long; the third bolt, at the same time presses the ends of two reinforced bar ladder beams and steel ladder beams to lower the reinforcement mesh. The surface of the roadway pillar surface is not less than 50 mm thick (as shown in Figure 14).

6.2. Observation Data Processing and Analysis. According to the results of a 50-day observation, the curves of the wall convergence and relative roof-to-floor convergence at the six observatories in the main retracement channel are plotted, as shown in Figures 16 and 17.

According to the observation of ground pressure, the deformation of the main withdrawal passage increases gradually with the advancing of the working face, but the increment is not great; the maximum deformation of roof and floor is 462 mm when the working face is connected; the maximum deformation of the two sides is 679 mm one day before the working face is connected.

7. Conclusion

In this paper, methods such as theoretical analysis, numerical calculation, and on-site monitoring were used to systematically study the key problem of retracement channel deformation on the fully mechanized caving working surface in superhigh seam, identifying the deformation mechanism of retracement channel. Main conclusions are as follows:

(1) The mechanical model for the retracement channel in thin bedrock, thick unconsolidated layer, and superhigh seam was established to get the deflection equation of the retracement channel. The calculated maximum deflection of the main retracement channel was 561 mm, meeting requirements for the working surface moving in the main retracement channel.

(2) Based on the calculation model of retracement channel established by FLAC^{3D} numerical

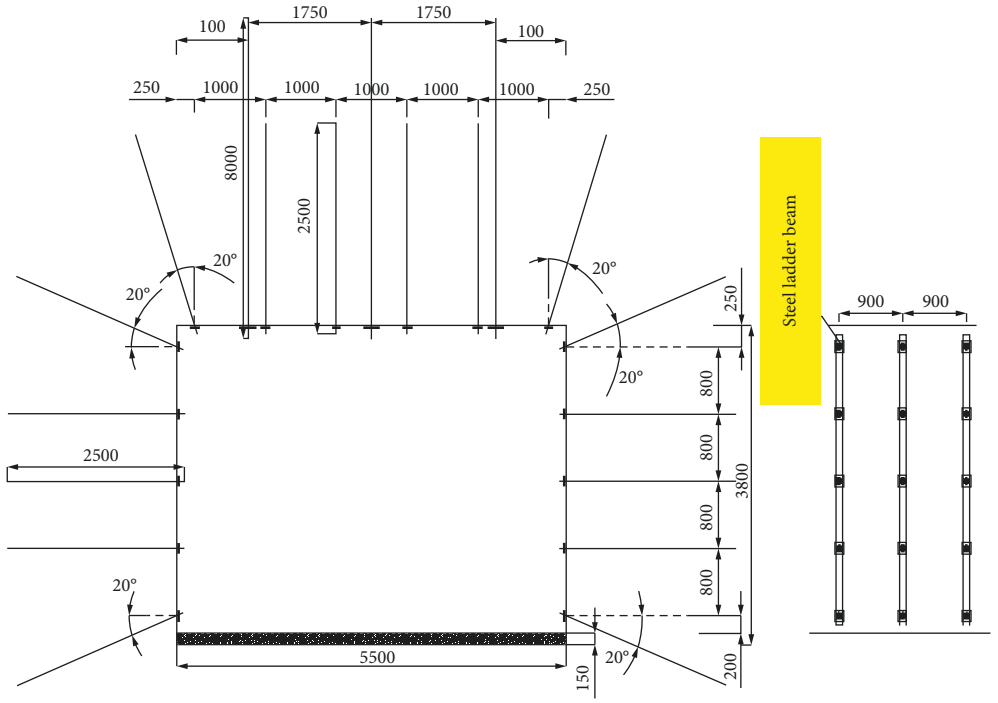

Figure 14: Schematic diagram of retracement laneway support.

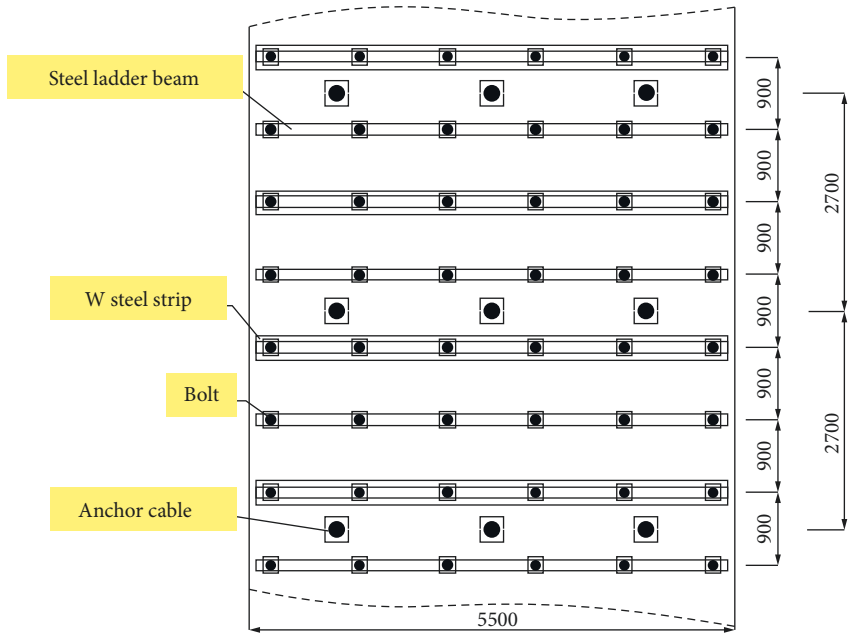

Figure 15: Schematic diagram of retracement laneway roof support.

calculation software, the stress and displacement distribution laws of rock surrounding the retracement channel during the end mining on the working surface under different surrounding schemes were analyzed to determine the optimal support schemes.

(3) The actual measurement shows that the optimal design scheme can effectively control the deformation of the rock surrounding the retracement channel during the end mining period. According to field monitoring, the maximum relative deformation of roof and floor of the main retracement channel during end mining is 462 mm, and the maximum wall convergence is 679 mm, far less than the allowable deformation for main retracement channel.

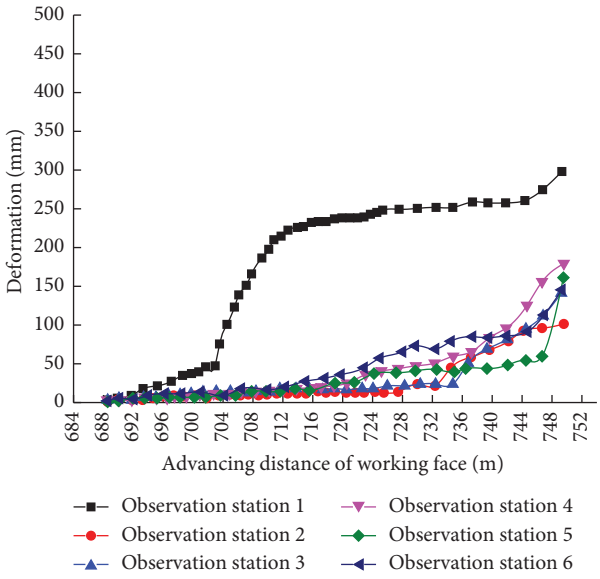

Figure 16: Roof-to-floor convergence of the main retracement laneway.

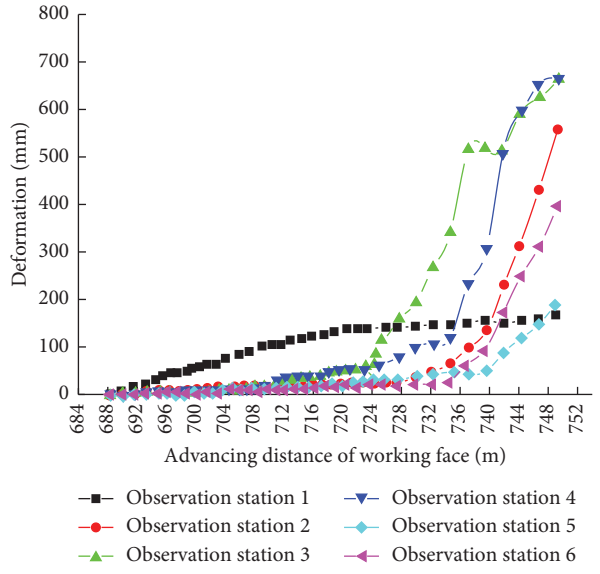

Figure 17: Wall convergence of the main retracement laneway.

Data Availability

The data used to support the findings of this study are available from the corresponding author upon request.

Conflicts of Interest

The authors declare no conflicts of interest.

Acknowledgments

This study was supported by the Key Scientific Research Projects of Suzhou College (no. 2017yzd15). We sincerely acknowledge the former researchers for their excellent research studies, which greatly assisted our academic study.

References

[1] Y.-G. Chen and M.-G. Qian, *Control of Surrounding Rock in China's Coal Mine Stope*, China University of Mining and Technology Press, Jiangsu Xuzhou, 1994.

[2] C.-L. Lai, *Practical Technology for High-Yield and High-Efficiency Mining of Thick Coal Seam*, Coal Industry Press, Beijing, China, 2001.

[3] Z.-W. Li, *Technology and Practical Experience of Caving Mining*, Coal Industry Press, Beijing, China, 1996.

[4] Y. Zhang, C. Li, Y. Si et al., "Influence of refuse content on economic benefits for fully mechanized top coal caving," *Procedia Engineering*, vol. 26, pp. 2391–2399, 2011.

[5] G. X. Xie, J. C. Chang, and K. Yang, "Investigations into stress shell characteristics of surrounding rock in fully mechanized top-coal caving face," *International Journal of Rock Mechanics and Mining Sciences*, vol. 46, no. 1, pp. 172–181, 2009.

[6] H. Alehossein and B. A. Poulsen, "Stress analysis of longwall top coal caving," *International Journal of Rock Mechanics and Mining Sciences*, vol. 47, no. 1, pp. 30–41, 2010.

[7] M. Khanal, D. Adhikary, and R. Balusu, "Evaluation of mine scale longwall top coal caving parameters using continuum analysis," *Mining Science and Technology (China)*, vol. 21, no. 6, pp. 787–796, 2011.

[8] S.-H. Tu, Y. Yong, Y. Zhen, X.-T. Ma, and W. Qi, "Research situation and prospect of fully mechanized mining technology in thick coal seams in China," *Procedia Earth and Planetary Science*, vol. 1, no. 1, pp. 35–40, 2009.

[9] L.-Q. Dang, F.-Q. Bao, and G.-H. Li, "Fully mechanized coal minning face equipment quickly moving from one surface practice," *Coal Mine machinery*, vol. 34, no. 12, pp. 182-183, 2013.

[10] M. M. Zdravkovich, "Different modes of Vortex shedding: an overview," *Journal of Fluids and Structures*, vol. 10, no. 5, pp. 427–437, 1996.

[11] C. H. K. William son, "Advances in our understanding of Vortex dynamics in bluff body wakes," *Journal of Wind Engineering and Industrial Aero dynamics*, vol. 7, pp. 69–71, 1997.

[12] M.-C. He and T. Peng, "The Problem of large deformation in softrock engineering and practical analysis of floor-heaving," *Journal of China University of Mining and Technology*, vol. 2, pp. 86–91, 1994.

[13] J. L. Luo, C. Haycocks, M. Karmis et al., "A new rock bolt design criterion and knowledge- based expert system for stratified roof," Dissertation, Virginia Polytechnic Institute and State University, Blacksburg, VA, USA, 1999.

[14] H. Lei, "Application of rapid removing equipment and technology for fully mechanized coal mining facen," *Coal Science and Technology*, vol. 36, no. 2, pp. 1–3, 2008.

[15] Y.-S. Xie, Q.-C. Wang, and B. Li, "Fast moving technique of working face in Shendong coal mining area," *Coal Mining Technology*, vol. 8, no. 3, pp. 49–51, 2008.

[16] G.-H. Wang, "Brief description of rapid relocation of fully mechanized coal mining face withdrawal channel in Shendong Mining Area," *Jiangxi Coal Science and Technology*, vol. 3, pp. 27-28, 2003.

[17] Y.-J. Wang, "Current situation and development trend conveyance of comprehensive mechanized of coal mining face equipment in China," *Coal Technology*, vol. 2, no. 4, pp. 7–9, 2010.

[18] Q. Ye, *Construction and Production Technology of Shendong Modern Mining Area*, China University of Mining and Technology Press, Jiangsu Xuzhou, China, 2002.
[19] J. Zhao, "Bolt support technology for large cross sectional equipment remove gateway and application," *Coal Science and Technology*, vol. 33, no. 11, pp. 5–7, 2005.
[20] Q. Li, Z.-D. Yan, S.-X. Liu, D.-X. Wang, M. Liu, and R.-S. Yang, "Research and practice on high efficiency continuous drivage for large cross section coal roadway," *China Mining Magazine*, vol. 15, no. 9, pp. 78–81, 2006.
[21] X.-W. Li and P.-Z. Ren, "Study on the network control observation method of roof behaviour in coal face," *Shangxi Mining Institute Learned Journal*, vol. 12, no. 3, pp. 245–249, 1994.
[22] Y.-S. Li and Y.-C. Liu, "Application of bolt and steel mesh support to equipment removing gateway of fully mechanized longwall coal mining face," *Coal Science and Technology*, vol. 38, no. 4, pp. 35-36, 2010.
[23] G.-l. Bai, J.-H. Gao, and G.-P. Wang, "Mining technology under highway of coal transportation in fully mechanized top-coal caving working face," *Metal Mine*, vol. 4, pp. 107–110, 2015.
[24] Y. Juan, S.-H. Tu, X.-G. Zhang, and B. Li, "System dynamics model of the support-surrounding rock system in fully mechanized mining with large mining height face and its application," *International Journal of Mining Science and Technology*, vol. 13, pp. 879–884, 2013.
[25] L. Yu, S.-B. Yan, H.-Y. Yu, and Z. Zhang, "Studying of dynamic bear characteristics and adaptability of support in top coal caving with great mining height," *Procedia Engineering*, vol. 26, pp. 640–646, 2011.
[26] Q.-M. Liu and D.-B. Mao, "Research on adaptability of full-mechanized caving mining with large mining-height," *Procedia Engineering*, vol. 26, pp. 652–657, 2011.
[27] P. Gong, Z. Ma, X. Ni, and R. R. Zhang, "An experimental investigation on the mechanical properties of gangue concrete as a roadside support body material for backfilling gob-side entry retaining," *Advances in Materials Science and Engineering*, vol. 2018, Article ID 1326053, 11 pages, 2018.
[28] P. Gong, Z. Ma, R. R. Zhang, X. Ni, and F. Liu, "An experimental investigation on the mechanical properties of gangue concrete as a roadside support body material for backfilling gob-side entry retaining," *Shock and Vibration*, vol. 2017, Article ID 6085941, 15 pages, 2017.